18TH WORLD CONFERENCE ON EARTHQUAKE ENGINEERING
WCEE2024
MILAN

MILAN, ITALY
30TH JUNE - 5TH JULY 2024
www.wcee2024.it

INNOVATIVE SETUP AND TESTING METHODOLOGY OF A NOVEL BIDIRECTIONAL ROTATION FRICTION DAMPER (BRFD)

E. Grossi[1*], R. De Risi[2], M. Zerbin[1], Flavia De Luca[2] & Alessandra Aprile[1]

[1] University of Ferrara, Ferrara, Italy, (*) eleonora.grossi@unife.it, corresponding author

[2] University of Bristol, Bristol, UK

Abstract: *Precast RC structures have been widely adopted for industrial and commercial buildings since the '60s in industrially developed countries. Precast RC structures with poor connections in earthquake-prone areas have a remarkable seismic risk due to the combined effect of high seismic vulnerability and exposure. Workers' safety requirements and the preservation of high-value facilities and stocks demand the adoption of effective retrofit techniques for earthquake risk mitigation and community resilience improvement. A novel device was patented in 2022, behaving as a frame beam-to-column joint and a damper with bidirectional dissipative capacity simultaneously. Very easy to install, low-cost and re-usable after the main shock, this Bidirectional Rotation Friction Damper (BRFD) has been designed to improve the seismic performance of such structures by excluding the brittle failure of structural and non-structural elements. Preliminary experimental tests performed at the University of Ferrara, Italy, proved the high-damping capacity of this novel device. Unlike usual dampers, the BRFD is subjected to actions in longitudinal and transversal directions and develops hysteresis cycles in both directions, making its experimental qualification peculiar. The object of this paper is the quality assessment of an ad hoc setup and testing methodology developed at the Heavy and Light Structure Lab of the University of Bristol (UK). Two orthogonal actuators have been coupled to apply displacement-force paths in two orthogonal directions. Forces, displacements and temperatures for different displacements, frequencies, and bolt preload levels were recorded. Results allowed the selection of the most appropriate testing methodology according to the expected real-use conditions for BFRDs under seismic actions.*

1. Introduction

The adoption of precast RC structures for industrial and commercial buildings spread out in industrially developed countries starting in the 60's, when seismic design regulations were rough, and buildings were mainly designed for gravity loads. The main issue of such structural typologies is the lack of effective connection between structural elements. As a result, precast RC structures with poor connections in earthquake-prone areas have a remarkable seismic risk due to the combined effect of high seismic vulnerability and exposure, as highlighted in the early 2000 state-of-the-art FIB report (International Federation for Structural Concrete 2003). The impact of this combined effect was also observed in the aftermath of the 2012 Northern Italy Earthquakes: a significant number of precast RC structures collapsed, resulting in 28 casualties, hundreds of injured persons, thousands displaced and massive damage to the regional economy (Bournas et al. 2014; Magliulo et al. 2014).

Workers' safety requirements and the preservation of high-value facilities and stocks demand the adoption of effective retrofit techniques for earthquake risk mitigation and community resilience improvement. Retrofit techniques based on energy dissipation devices have proved to be very efficient, preventing damage to structural elements (Christopoulos & Filatrault 2006), and an economical solution if compared to the traditional techniques (Grossi et al. 2020; Zerbin & Aprile 2015; Zhang et al. 2023).

Several studies on precast RC frames suggested the adoption of post-installed connection devices between structural elements acting as dampers as well (Belleri et al. 2017; Eldin et al. 2020; Martinelli & Mulas 2010), resulting in a quite promising solution. These devices exhibited good structural performance in terms of both energy dissipation and interstorey drifts reduction. However, these beneficial effects were limited to the direction along which these devices are installed. Moreover, adding damping in all horizontal directions is not achievable if the building lacks a 3D structural configuration.

The authors developed a novel device that simultaneously behaves as a beam-to-column joint and a damper with bidirectional dissipative capacity. Very easy to install, low-cost and re-usable after the main shock, this Bidirectional Rotation Friction Damper (BRFD) has been designed to improve the seismic performance of industrial structures by excluding the brittle failure of structural and non-structural elements (Aprile et al. 2023). Preliminary experimental tests performed at the University of Ferrara, Italy, have proved the high-damping capacity of this novel device (Grossi et al., submitted). Unlike usual dampers, the BRFD is subjected to actions in longitudinal and transversal directions and develops hysteresis cycles in both directions, making its experimental qualification non-straightforward.

This paper shows a part of the main findings of an experimental campaign whose object is the quality assessment of an ad hoc setup and testing methodology developed at the Heavy and Light Structure Lab of the University of Bristol (UK). Section 2 describes the BRFD structural layout and briefly highlights the preliminary findings. Section 3 describes the experimental setup, while Section 4 shows the main results and discussions. The final Section 5 collects the main findings and remarks.

2. The BRFD layout

Starting conceptually from a Rotational Friction Damper (RFD) and using a movable plate geometry, the BRFD consists of multiple layers of steel plates whose contact surfaces dissipate energy by friction, as shown in the axonometric view of Figure 1(a). The connection to the existing frame is executed at the beam-to-column joints level with an inclination angle of about 45° from the longitudinal beam axis (see Figure 1(b)), depending on the available space, fixing the ends of the BRFD to both beam and column.

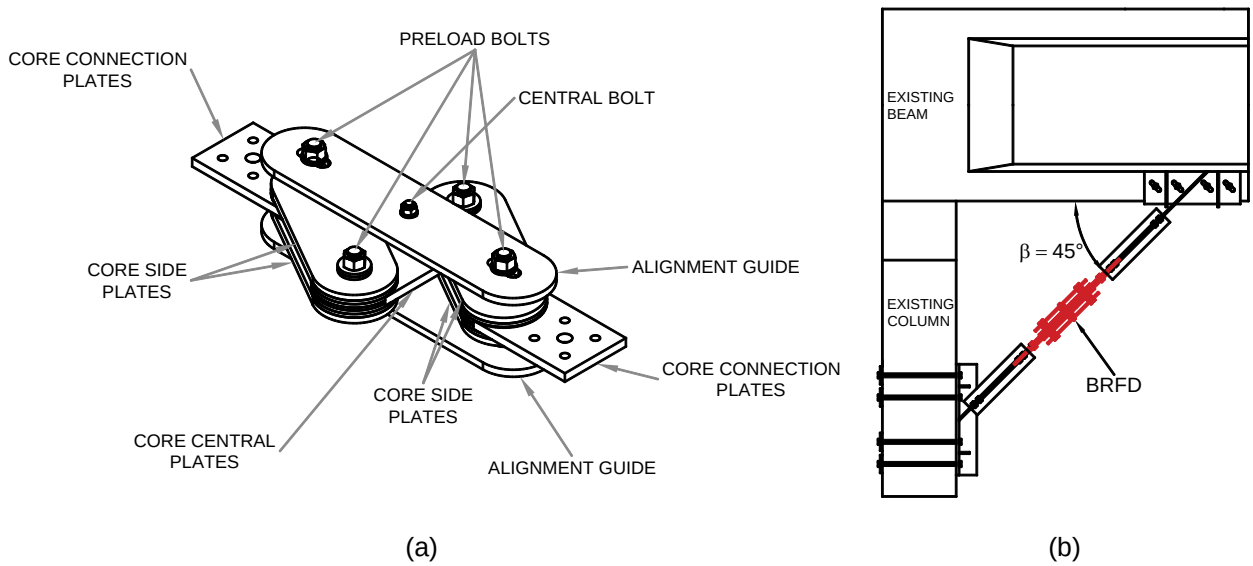

Figure 1. BRFD (a) axonometric view and (b) frame connection example.

Core plates and core connection plates are the main elements of the BRFD and are kept coupled by four preload stud bolts. The geometry and the mechanical properties of these main elements highly influence the

BRFD activation force and initial stiffness. Following suggestions from the literature (Grigorian et al. 1993; Latour et al. 2014), Belleville spring washers are used to avoid the loss of bolt tension during cyclic excitations. A two-in-series configuration has been adopted for each stud bolt.

As the BRFD activates, core central and side plates rotate around the preload stud bolts, dissipating energy thanks to the friction generated by the plates' contact (see the coloured areas of Figure 2). At the top and the bottom of the BRFD two guides with slotted holes are placed to maintain the preload stud bolts of core connection plates lined up with the central stud bolt. It is worth noting that the movable geometry of the BRFD allows a two-component displacement, as shown in Figure 2. A general displacement can be decomposed into a longitudinal component dx and a transversal component dy. Consequently, the BRFD's activation force has two components: a longitudinal component $F_{act,L}$ (x direction) and a transversal component $F_{act,T}$ (y direction). Moreover, the energy dissipation occurs in correspondence of the blue area (see Figure 2) for longitudinal displacements and in correspondence of the red area (see Figure 2) for transversal displacements.

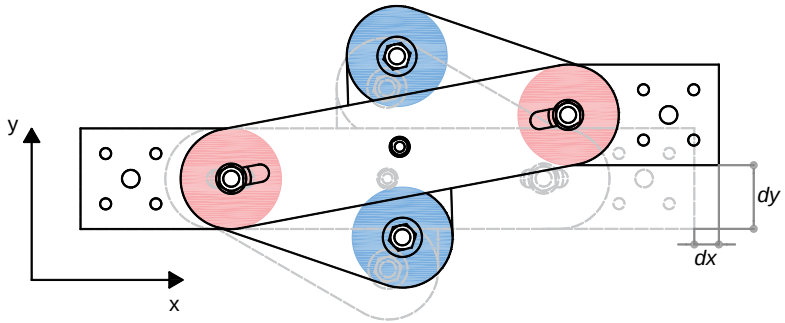

Figure 2. BRFD bidirectional deformed shape.

The design of the BRFD prototype first requested the selection of proper coupling materials which can develop a reliable and steady friction coefficient μ. A preliminary tribological investigation was performed at the Metallurgy Laboratory (Engineering Department, University of Ferrara, Italy) (Grossi, Aprile and Zerbin, 2023; Grossi *et al.*, 2023) to compare the effects of different surface finishing and treatments on the steadiness of μ. Of all the investigated surfaces, nickel coated steel and bronze were identified as suitable materials.

First mechanical tests were performed at the Structural Integrity Laboratory (Engineering Department, University of Ferrara, Italy) (Grossi et al., submitted). However, the adopted experimental setup allowed the execution of longitudinal tests only and did not allow the measurement of the stress in the stud bolts. Therefore, it was clear the necessity of performing tests in both longitudinal and transversal directions and measuring the stud bolts axial tension.

3. Experimental setup and methodology

The BRFD prototype has been manufactured using S355JR structural steel (CEN 2015a), using four M16 class 12.9 (CEN 2015b) preload stud bolts and one M12 class 12.9 (CEN 2015b) central stud bolts. The coupling nickelled steel vs. bronze (NB) has been selected as a friction interface for this investigation. The overall dimension of the prototype is 70x30x20 cm. Nuts have been tightened using a FERVI 0803/S210 manual torque wrench (FERVI SpA, Modena, Italy) to ensure the application of constant tension to the stud bolts. The torquing procedure followed the torque method, suggested as the most accurate among all the standardized methods (Ferrante Cavallaro et al. 2018).

The mechanical tests were performed at the Heavy and Light Structure Lab of the University of Bristol (UK). Two 25 kN Instron actuators have been coupled to activate the BRFD in longitudinal and transversal directions, as shown in Figure 3. Three M16 stud bolts have been instrumented by installing BTMC bolt strain gauges (Tokyo Measuring Instruments Laboratory Co., Ltd., Tokyo, Japan) to measure the bolt's axial tension during the tests. Two horizontal LVDTs with a maximum displacement of 100 mm have been placed to double-check the displacements imposed by the actuators, and two vertical LVDTs with a maximum displacement of 10 mm have been used to check the vertical displacement of the device during the tests. Four type-K thermocouples have been placed close to the BRFD's friction interface to measure the temperature increment in the proximity

of the dissipating area, assessing the amount and the effects of the temperature increment on the BRFD behaviour.

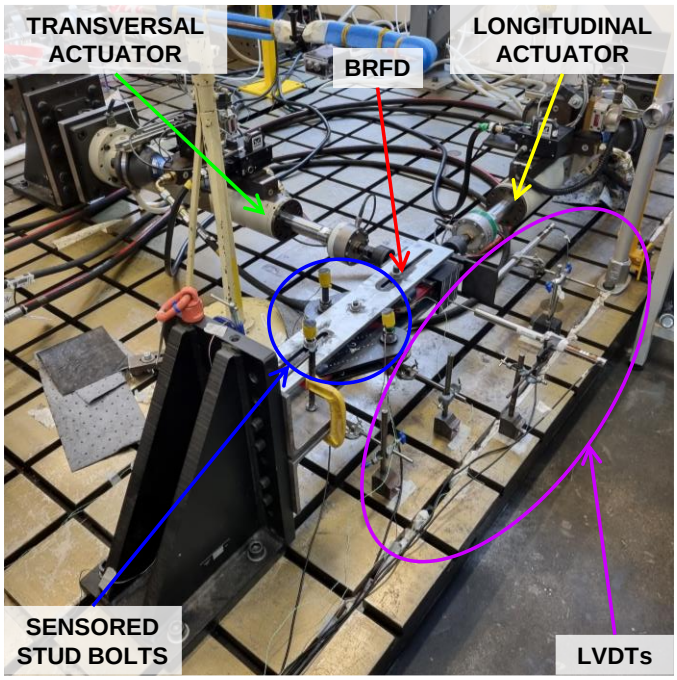

Figure 3. Experimental setup and main adopted sensors.

The testing protocol has been defined according to EN 15129 (CEN 2018) and the main findings from the preliminary tests performed (Grossi et al., submitted). Two test groups have been defined: Group 1 (G1) tests aimed at assessing the BRFD behaviour in the real-use condition. Group 2 (G2) tests aimed at determining the relationship between the coefficient of friction and the velocity to calibrate a numerical model. More precisely, G1 tests have been performed using a sinusoidal displacement law incrementing the displacement amplitude every ten cycles (±10, ±20, ±40 mm) and investigating four different frequencies (0.05 Hz, 0.50 Hz, 1.00 Hz and 2.00 Hz, respectively tagged as F1, F2, F3 and F4). G2 tests have been performed using a triangular displacement law with fixed ±20 mm displacement amplitude and incrementing the frequency every five cycles from 0.05 Hz to 2.00 Hz in six steps. G1 and G2 tests have been performed separately in longitudinal (L) and transversal direction (T). Two different toque levels have been applied, 50 Nm (T1) and 75 Nm (T2), which correspond to an axial tension of 20 kN and 35 kN respectively.

To increase the steadiness of the overall BRFD behaviour, a 300 s running-in has been performed in both longitudinal and transversal directions before the actual tests and using a sinusoidal displacement law at a frequency of 0.50 Hz and fixed ±20 mm displacement amplitude.

Because of the experimental setup limits, the transversal component has been activated only partially: in fact, to obtain the BRFD's deformation of Figure 2, both ends of the device need to be fixed. On the contrary, the BRFD end connected to the actuators has been hinged for the safety of the equipment, resulting in a slight change of the BRFD static scheme for the transversal component.

4. Test results and discussion

4.1. G1 tests

Hysteretic cycles

Figure 4 and Figure 5 show the recorded hysteresis of the BRFD during G1 tests with T1 and T2 torque levels, respectively. When the device is subjected to longitudinal displacements (see Figure 4(a) and Figure 5(a)), the hysteresis cycle shape is mainly rectangular, with a slight pinching effect in correspondence with the reverse-motion point. On the contrary, when the device is subjected to transversal displacements (see Figure 4(b) and Figure 5(b)), the pinching effect is more visible, especially for larger displacements. This difference in shape can be explained by considering the combination of geometrical effects and experimental setup configuration.

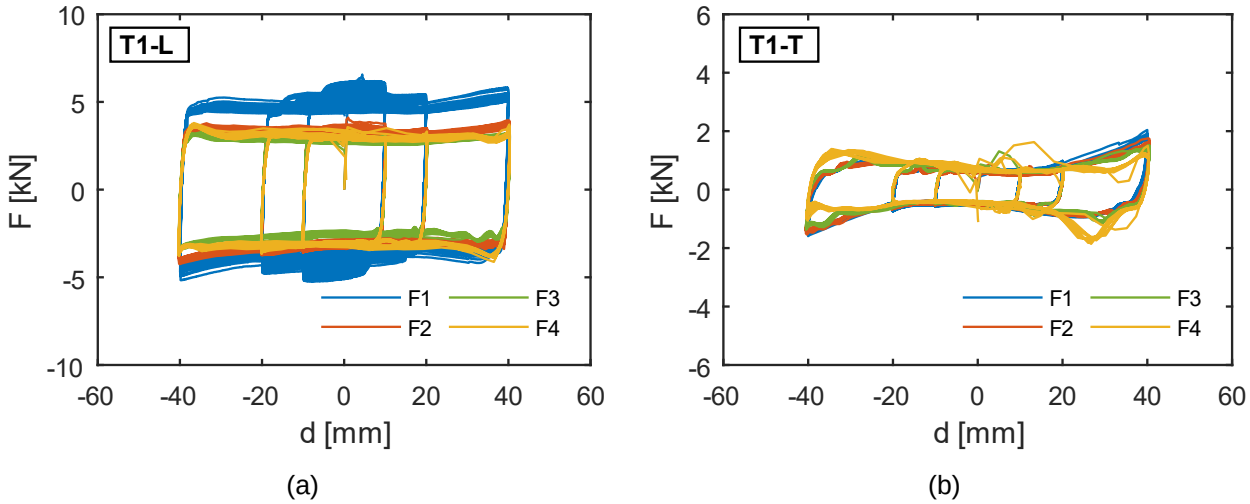

Figure 4. Recorded hysteresis cycles for T1 torque (50 Nm) in (a) longitudinal and (b) transversal direction.

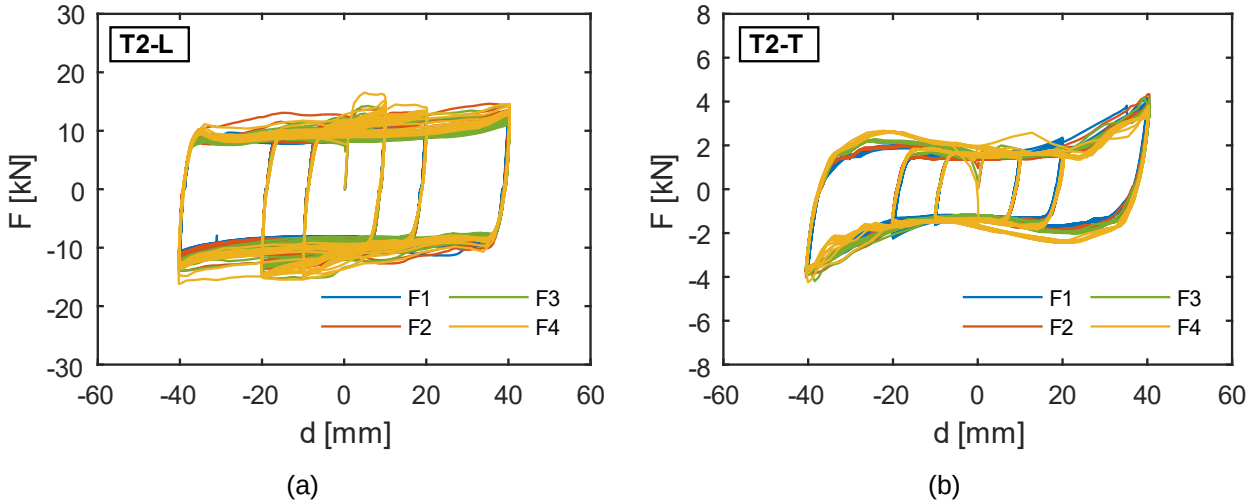

Figure 5. Recorded hysteresis cycles for T2 torque (75 Nm) in (a) longitudinal and (b) transversal direction.

Concerning the investigated torque levels, the increment of torque registers an increment of overall forces in both longitudinal and transversal directions. Independent of the applied torque level, the oscillation frequency does not affect the overall behaviour in the two directions, with similar loop shapes and recorded forces from F1 to F4.

Activation and maximum forces

Two different average forces are calculated to highlight the steadiness and repeatability of the hysteresis cycles. The activation force F_{act} is the average force at zero-displacements, while the maximum force F_{max} is the average force at maximum displacements. Figures 6 compares F_{act} and F_{max} in longitudinal and transversal directions for T1 and T2 torque levels. For both the investigated torque levels and displacement directions, F_{max} values are higher than F_{act}; the two values are not particularly affected by the frequency increment; however, the difference between F_{act} and F_{max} increases as the frequency increases.

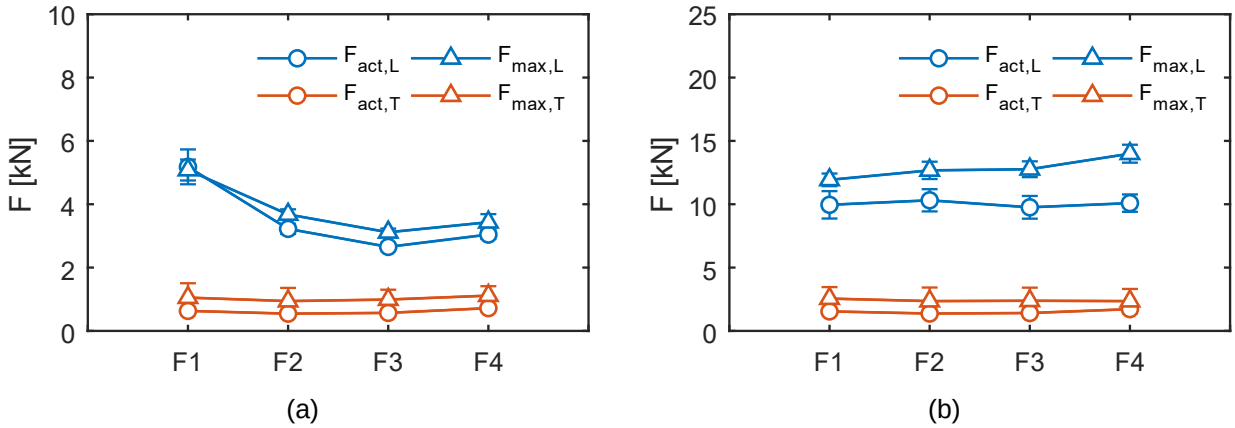

Figure 6. Comparison between F_{act} and F_{max} in L and T directions for (a) T1 and (b) T2 torque levels.

When T1 torque level is applied, $F_{act,L}$ averages 3.52 kN and $F_{max,L}$ 3.83 kN with an average increment of 11% from $F_{act,L}$ to $F_{max,L}$, while $F_{act,T}$ averages 0.62 kN and $F_{max,T}$ 1.02 kN with an average increment of 67% from $F_{act,T}$ to $F_{max,T}$. The average coefficient of variation of $F_{act,L}$ and $F_{act,T}$ is almost 6% for both directions. When T2 torque level is applied, $F_{act,L}$ averages 10.03 kN and $F_{max,L}$ 12.84 kN with an average increment of 28% from $F_{act,L}$ to $F_{max,L}$, while $F_{act,T}$ averages 1.51 kN and $F_{max,T}$ 2.41 kN with an average increment of 61% from $F_{act,T}$ to $F_{max,T}$. The average coefficient of variation of $F_{act,L}$ is 9% and of $F_{act,T}$ is 6%.

Both the investigated torque levels register a higher average increment from F_{act} to F_{max} in the transversal direction, confirming the pinching effect observed in the hysteresis cycles (see Figure 4(b) and Figure 5(b)). The increment from F_{act} to F_{max} in the longitudinal direction is less remarkable, confirming the presence of a more rectangular hysteresis loop shape. Concerning the steadiness of the hysteresis cycles, the coefficient of variation of F_{act} is computed. It is about 7% in the longitudinal direction and 6% in the transversal direction, highlighting a quite remarkable steadiness of the hysteresis cycle in both directions.

Equivalent damping coefficient

To assess the efficiency of the BRFD in the real use condition, the equivalent damping coefficient is estimated using the Jacobsen formulation (Jacobsen 1965), which can be written as:

$$\xi_{eq,hyst} = \frac{EDC}{2\pi d_{max} F_{max}} \tag{1}$$

where EDC is the energy dissipated per cycle, while d_{max} and F_{max} are the maximum displacement and force reached during the cycle.

Eq. (1) is applied to each recorded cycle, and Figure 7 shows the average values as a function of the frequency for both T1 and T2 torque levels. The increment of torque level and frequency does not affect the overall values; however, in transversal direction $\xi_{eq,hyst}$ is more variable.

When the T1 torque level is applied, $\xi_{eq,hyst,L}$ averages 55% with a coefficient of variation of 4%, while $\xi_{eq,hyst,T}$ averages 42% with a coefficient of variation of 20%. When the T2 torque level is applied, $\xi_{eq,hyst,L}$ averages 48% with a coefficient of variation of 4%, while $\xi_{eq,hyst,T}$ averages 43% with a coefficient of variation of 22%.

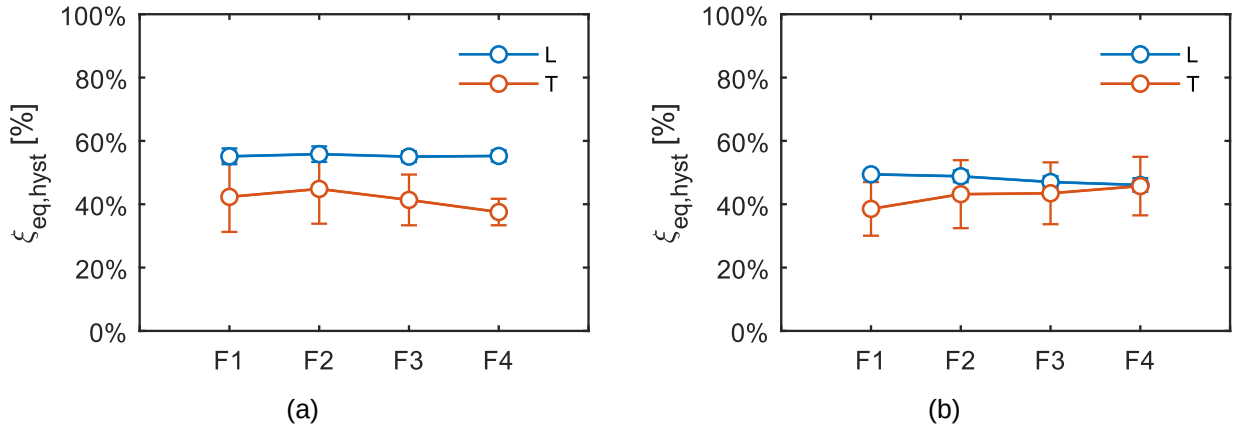

Figure 7. Equivalent damping coefficient in L and T directions for (a) T1 and (b) T2 torque levels.

As previously remarked, $\xi_{eq,hyst,T}$ register a higher variation with respect to $\xi_{eq,hyst,L}$ for both T1 and T2 torque levels. This difference is strictly related to the hysteresis loop shapes. In the longitudinal direction, the shape is almost rectangular as it is unaffected by the displacement amplitude increment (see Figure 4(a) and Figure 5(b)). In the transversal direction, the shape is highly affected by the displacement amplitude increment (see Figure 4(b) and Figure 5(b)). More precisely, in the transversal direction, the hysteresis loop shape is more rectangular for smaller displacement and more trapezoidal for bigger displacement. As a result, the transversal direction registers higher $\xi_{eq,hyst}$ values for smaller cycles and smaller $\xi_{eq,hyst}$ values for bigger cycles, decreasing the overall steadiness. On the contrary, the longitudinal direction registers similar $\xi_{eq,hyst}$ values for smaller and bigger cycles, increasing the overall steadiness.

4.2. G2 tests

Hysteresis cycles

Figure 8 shows the recorded hysteresis cycles of the BRFD during G2 tests with T1 and T2 torque levels. When the device is subjected to longitudinal and transversal displacements, the hysteresis cycle shape is rectangular, with a slight pinching effect corresponding to the reverse-motion point. This behaviour slightly differs from the one observed during G1 tests, especially in the transversal direction. In fact, during G2 tests, the pinching effect in the transversal direction is less remarkable. This difference is caused by the smaller displacement amplitude, which decreases the geometric effects, and the type of displacement law, which ensures a constant sliding velocity.

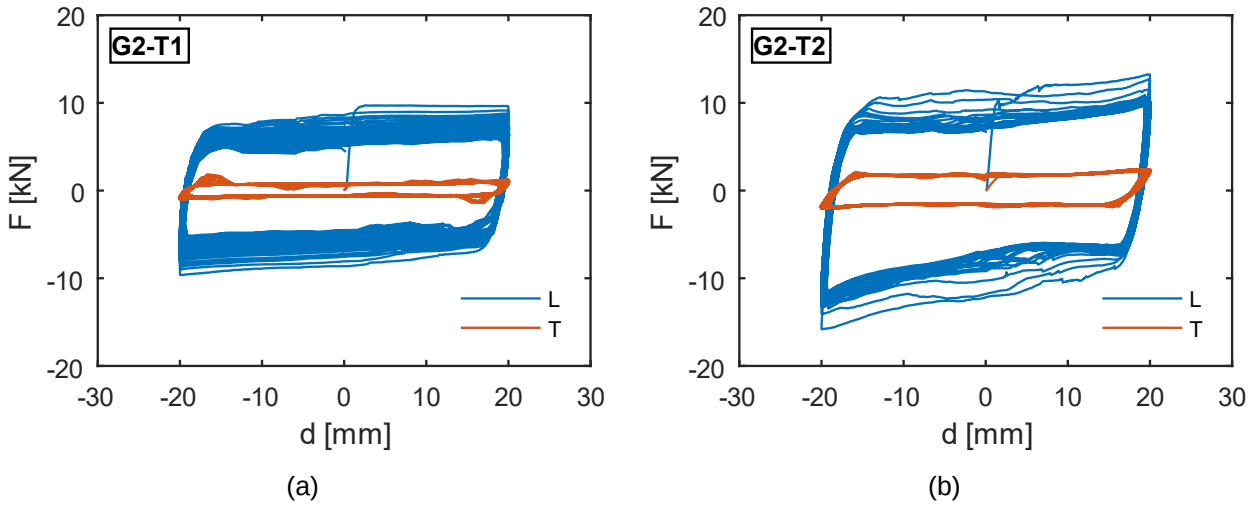

Figure 8. G2 tests recorded hysteresis cycles in L and T directions for (a) T1 and (b) T2 torque levels.

Concerning the force values, the recorded forces decrease with sliding velocity increment when the BRFD is subjected to longitudinal displacement. On the contrary, when the BRFD is subjected to transversal displacement, the recorded forces remain almost constant with sliding velocity increment.

When the T1 torque level is applied, $F_{act,L}$ averages 6.41 kN with a coefficient of variation of 3%, while $F_{act,T}$ averages 0.71 kN with a coefficient of variation of 2%. When the T2 torque level is applied, $F_{act,L}$ averages 7.71 kN with a coefficient of variation of 3%, while $F_{act,T}$ averages 1.67 kN with a coefficient of variation of 2%. These values slightly differ from the ones registered during G1 tests. Still, this difference can be explained by the different bolt axial tension reached during the application of the torque from one test to the other.

Coefficient of friction evaluation

The evaluation of the dynamic friction coefficient μ in a friction device is extremely important for its experimental qualification and numerical implementation. In this work, μ has been computed using two different approaches: the first one uses analytical relationships, and the second one uses the dissipated energy per cycle (EDC), according to the standards EN 15129 (CEN 2018). These two approaches are then compared to assess the analytic model. Furthermore, since the BRFD is a rotational friction damper, the evaluation of the friction coefficient can be computed referring to the rotational mechanism of the friction interface and the overall BRFD behaviour.

Considering the rotational mechanism of the friction interface, when the BRFD activates, core central and side plates rotate around the preload stud bolts, as previously discussed in Section 2. This means that the plates start rotating when their ends reach a certain value of moment, called sliding moment M_s, which can be defined under the hypothesis of uniform contact as follows (Belleri et al. 2017):

$$M_s = n\int_{\rho=R_i}^{R_e}\int_{\theta=0}^{2\pi}\rho^2\frac{\mu_r F_P}{\pi\left(R_e^{\,2}-R_i^{\,2}\right)}d\rho d\theta = n\mu_r F_P\frac{2}{3}\frac{R_e^{\,3}-R_i^{\,3}}{R_e^{\,2}-R_i^{\,2}} = n\mu_r F_P r_{eq} \tag{2}$$

where n is the number of friction interfaces, μ_r is the interface's friction coefficient associated with the rotational mechanism, F_P is the stud bolt preload, R_e and R_i are the outer and inner contact area radius, respectively, and ρ and θ are the radial and angular coordinates respectively. The ratio between R_e and R_i can be simplified using r_{eq} as an equivalent radius.

The activation forces in longitudinal and transversal directions, $F_{act,L}$ and $F_{act,T}$, respectively, of the BRFD inside the experimental setup, are computed using Eq. (3), where l_1 is the distance between the stud bolts, and l_2 is an additional distance to consider the connection point of the transversal actuator.

$$F_{act,L} = \frac{2M_s}{l_1}; \quad F_{act,T} = \frac{M_s}{\sqrt{3}l_1 + l_2} \tag{3}$$

The values of μ_r are computed by joining Eqs. (2) and (3) starting from $F_{act,L}$ and $F_{act,T}$.

$$\mu_{r,L} = \frac{M_s}{F_P r_{eq} n} = \frac{F_{act,L} l_1}{2F_P r_{eq} n}; \quad \mu_{r,T} = \frac{M_s}{F_P r_{eq} n} = \frac{F_{act,T}\left(\sqrt{3}l_1 + l_2\right)}{2F_P r_{eq} n} \tag{4}$$

The overall BRFD behaviour can be simplified as a simple flat slider resembling a friction isolation system with n friction interfaces subjected to an F_P vertical load. Under these hypotheses, Eq. (3) can be written as:

$$F_{act,L} = \mu_{l,L} n F_P; \quad F_{act,T} = \mu_{l,T} n F_P \tag{5}$$

where $\mu_{l,L}$ and $\mu_{l,T}$ are the BRFD friction coefficients associated to the overall linear behaviour along longitudinal and transversal directions, respectively. The values of $\mu_{l,L}$ and $\mu_{l,T}$ are computed by joining Eqs. (2), (3) and (5) starting from $F_{act,L}$ and $F_{act,T}$; moreover, $\mu_{l,L}$ and $\mu_{l,T}$ are describable as a function of μ_r as follows:

$$\mu_{l,L} = \frac{2\mu_r r_{eq} n}{l_1}; \quad \mu_{l,T} = \frac{\mu_r r_{eq} n}{\sqrt{3}l_1 + l_2} \tag{6}$$

The formulation suggested by the standard EN 15129 (CEN 2018) refers to friction isolators and has been successfully adopted in several experimental investigations (Furinghetti et al. 2019; Pavese et al. 2018) to evaluate the coefficient of friction starting from force-displacement hysteresis cycles ($EDC_{F,d}$). Adapting the

formulation of EN15129 to the BRFD's overall linear behaviour, the linear friction coefficient is computed using Eq. (7), where d_{max} is the maximum displacement reached during the hysteresis cycle.

$$\mu_{EDC,l} = \frac{EDC_{F,d}}{4 d_{max} F_P} \tag{7}$$

Adopting the same approach to compute the friction coefficient associated with the rotational mechanism, Eq. (7) is modified considering the EDC associated with the hysteresis cycles expressed as moment-rotation relationship ($EDC_{M,\theta}$) obtaining Eq. (8), where θ_{max} is the maximum rotation reached during the hysteresis cycle.

$$\mu_{EDC,r} = \frac{EDC_{M,\theta}}{4 \theta_{max} F_P n r_{eq}} \tag{8}$$

It is worth noting that because of the nature of the BRFD, the evaluation of the rotational coefficient of friction μ_r in longitudinal and transversal directions is expected to show similar values between the two directions. In fact, μ_r is strictly associated with the friction interface properties of the device, which is the same in both directions. On the contrary, the evaluation of the linear coefficient of friction μ_l in longitudinal and transversal directions is expected to show different values between the two directions. In fact, μ_l is strictly associated with the overall BRFD behaviour, which differs for longitudinal and transversal directions.

Relationship between friction coefficient and sliding velocity

The friction coefficients are evaluated according to the above procedure in both longitudinal (L) and transversal (T) directions.

Figure 9 shows the relationship between the linear coefficient of friction and sliding velocity for both T1 and T2 torque levels, comparing the results obtained using the analytical and EDC approaches. The friction coefficient decreases for both the applied torque levels as the sliding velocity increases, especially along the L direction.

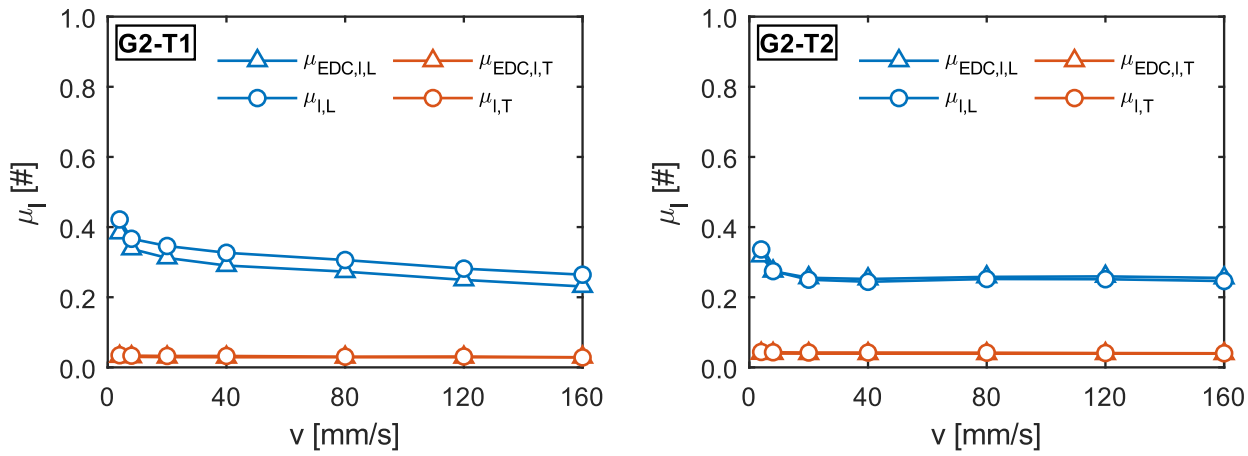

Figure 9. Linear coefficient of friction comparison in L and T directions for (a) T1 and (b) T2 torque levels.

When the T1 torque level is applied, $\mu_{l,L}$ averages 0.33 and $\mu_{EDC,l,L}$ 0.30 with an average difference of 10%, while $\mu_{l,T}$ averages 0.032 and $\mu_{EDC,l,T}$ 0.029 with an average difference of 7%. When the T2 torque level is applied, $\mu_{l,L}$ averages 0.265 and $\mu_{EDC,l,L}$ 0.267 with an average difference of 0.01%, while $\mu_{l,T}$ averages 0.042 and $\mu_{EDC,l,T}$ 0.039 with an average difference of 7%.

As expected, the linear coefficient of friction is significantly different for L and T, with a difference in percent of about 87%. On the contrary, the values obtained using the two approaches are similar for both T1 and T2 torque levels, with a difference between the μ_l and $\mu_{EDC,l}$ that decreases when increasing the torque level, going from 9% to 3% from T1 to T2.

Figure 10 shows the relationship between the rotational coefficient of friction and rotational sliding velocity for both T1 and T2 torque levels, comparing the results obtained using the analytical and EDC approaches. The

friction coefficient decreases for both the applied torque levels as the sliding velocity increases, especially along the L direction.

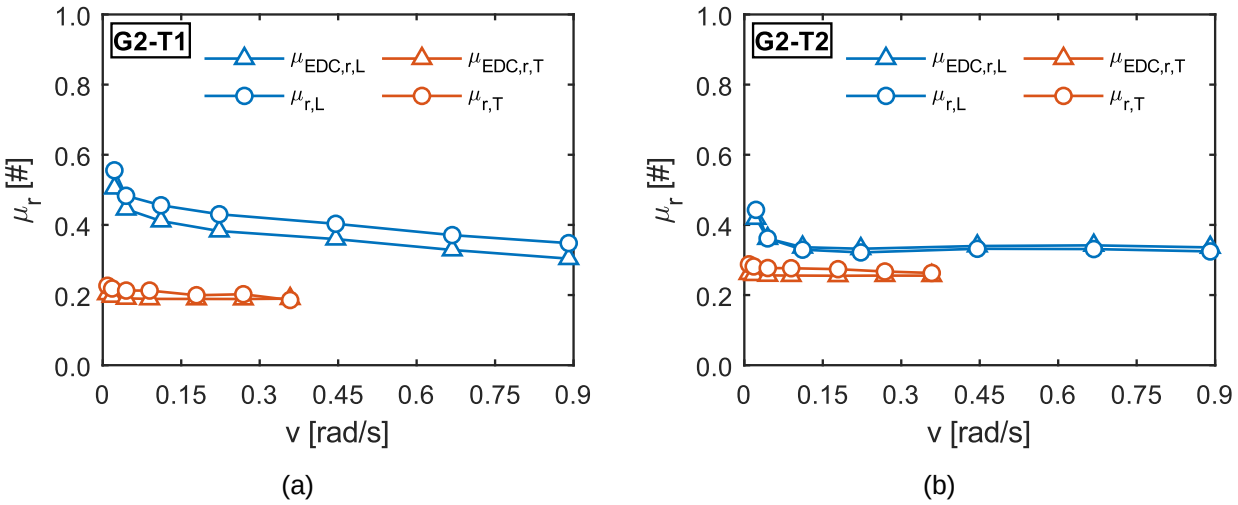

Figure 10. Rotational coefficient of friction comparison in L and T directions for (a) T1 and (b) T2 torque levels.

When the T1 torque level is applied, $\mu_{r,L}$ averages 0.44 and $\mu_{EDC,r,L}$ 0.39 with an average difference of 10%, while $\mu_{r,T}$ averages 0.21 and $\mu_{EDC,r,T}$ 0.19 with an average difference of the 8%. When T2 torque level is applied, $\mu_{r,L}$ averages 0.349 and $\mu_{EDC,r,L}$ 0.352 with an average difference of the 1%, while $\mu_{r,T}$ averages 0.28 and $\mu_{EDC,r,T}$ 0.26 with an average difference of the 7%.

As expected, the rotational coefficient of friction is similar for L and T compared to the linear ones. However, the difference between L and T is still large but decreases with the torque level increment, going from a 51% to a 24% difference from T1 to T2. On the contrary, the values obtained using the two approaches are similar for both for T1 and T2 torque levels, with a difference between the μ_r and $\mu_{EDC,r}$ that decreases when increasing the torque level, going from 9% to 3% from T1 to T2.

5. Conclusions

The present work shows a part of the main findings of an experimental campaign whose object is the quality assessment of an ad hoc setup and testing methodology for the mechanical characterization of a novel bidirectional friction damper. The experimental setup and testing methodology have been developed at the Heavy and Light Structure Lab of the University of Bristol, UK, by coupling two actuators to perform mechanical tests in two directions. The testing protocol has been defined according to EN 15129 (CEN 2018) and the main findings from the preliminary tests performed at the Structural Integrity Laboratory of the University of Ferrara, Italy (Grossi et al., submitted). Two test groups were defined: G1 tests focused on the assessment of the BRFD behaviour in the real-use condition, while G2 tests focused on the definition of the relationship between the coefficient of friction and the velocity to calibrate a numerical model. The tests have been performed in both longitudinal and transversal directions characterising the two main displacement components of the BRFD. The main findings are following summarised:

- The experimental setup cannot fully reproduce the BRFD's real use constraints, especially for the transversal component. As a result, the experimental setup has partially exploited the BFRD's transversal damping capacity.
- The hysteresis cycles differ from the longitudinal and transversal directions regarding developed forces and loop shape. These differences are due to the BRFD itself, which reaches higher forces in the longitudinal direction, and to the experimental setup limitations, which modify the BRFD transversal response, developing a pinching effect when reaching larger displacements.

- The BRFD exhibits hysteresis cycles with a high steady and repeatable behaviour in both longitudinal and transversal directions. Moreover, the frequency increment does not compromise the stability of the hysteresis cycles, registering a coefficient of variation of the activation force of about 7% for the longitudinal direction and 6% for the transversal direction.
- The computed equivalent damping is about 52% in the longitudinal direction and 43% in the transversal direction, highlighting the presence of a rectangular hysteresis loop shape.
- The relationship between the coefficient of friction and sliding velocity shows that the friction coefficient slightly decreases as the sliding velocity increases.
- The friction coefficient computed using the analytical and EDC approach shows extremely similar results, validating the two adopted methodologies. Moreover, the evaluation of the rotational coefficient of friction μ_r, can be used as an indicator for developing a uniform contact in the friction interface.
- The application of a higher torque level increases the interface contact uniformity and increases the similarity between L and T in terms of BRFD overall performance.

Further steps of the experimental activity are reviewing the experimental setup to fully reproduce the BRFD's real use condition in the transversal direction and the execution of bidirectional tracks.

6. References

Aprile A, Grossi E, Zerbin M. 2023. A Novel Friction Damper for Seismic Retrofit of Precast RC Structures with Poor Connections. *Fib Symposium 2023 - Building for the Future: Durable, Sustainable, Resilient - Volume 1*, pp. 1384–94

Belleri A, Marini A, Riva P, Nascimbene R. 2017. Dissipating and re-centring devices for portal-frame precast structures. *Eng Struct*. 150:

Bournas DA, Negro P, Taucer FF. 2014. Performance of industrial buildings during the Emilia earthquakes in Northern Italy and recommendations for their strengthening. *Bulletin of Earthquake Engineering*. 12(5):

CEN. 2015a. *Hot rolled products of structural steels - Part 1: General technical delivery conditions (UNI EN 10025-1:2005)*

CEN. 2015b. *High-strength structural bolting assemblies for preloading - Part 1: General requirements (UNI EN 14399-1:2015)*

CEN. 2018. *Anti-seismic devices (UNI EN 15129:2018)*

Christopoulos C, Filatrault A. 2006. *Principles of Passive Supplemental Damping and Seismic Isolation*. Pavia, Italy: IUSS Press

Eldin MN, Dereje AJ, Kim J. 2020. Seismic retrofit of RC buildings using self-centering PC frames with friction-dampers. *Eng Struct*. 208:

Ferrante Cavallaro G, Latour M, Francavilla AB, Piluso V, Rizzano G. 2018. Standardised friction damper bolt assemblies time-related relaxation and installed tension variability. *J Constr Steel Res*. 141:145–55

Furinghetti M, Pavese A, Quaglini V, Dubini P. 2019. Experimental investigation of the cyclic response of double curved surface sliders subjected to radial and bidirectional sliding motions. *Soil Dynamics and Earthquake Engineering*. 117:190–202

Grigorian CE, Yang TS, Popov EP. 1993. Slotted Bolted Connection Energy Dissipators. *Earthquake Spectra*. 9(3):

Grossi E, Aprile A, Zerbin M, Livieri P. Preliminary Experimental Tests of a Novel Friction Damper for Seismic Retrofit of RC Precast Structures. *Engineering Structures (in review)*

Grossi E, Zerbin M, Aprile A. 2020. Advanced Techniques for Pilotis RC Frames Seismic Retrofit: Performance Comparison for a Strategic Building Case Study. *Buildings*. 10(9):149

International Federation for Structural Concrete. 2003. *Seismic Design of Precast Concrete Building Structures: State-of-Art Report*, Vol. 27. Lausanne: fib

Jacobsen LS. 1965. Damping in composite structures. *2nd World Conference on Earthquake Engineering, Vol. 2*, pp. 1029–44. Tokyo: Science Council of Japan

Latour M, Piluso V, Rizzano G. 2014. Experimental analysis on friction materials for supplemental damping devices. *Constr Build Mater*. 65:

Magliulo G, Ercolino M, Petrone C, Coppola O, Manfredi G. 2014. The Emilia Earthquake: Seismic Performance of Precast Reinforced Concrete Buildings. *Earthquake Spectra*. 30(2):

Martinelli P, Mulas MG. 2010. An innovative passive control technique for industrial precast frames. *Eng Struct*. 32(4):

Pavese A, Furinghetti M, Casarotti C. 2018. Experimental assessment of the cyclic response of friction-based isolators under bidirectional motions. *Soil Dynamics and Earthquake Engineering*. 114:1–11

Zerbin M, Aprile A. 2015. Sustainable retrofit design of RC frames evaluated for different seismic demand. *Earthquakes and Structures*. 9(6):1337–53

Zhang Y, De Risi R, Alexander NA. 2023. The Sliding Keys on Inclined Deflecting-cantilevers (SKID) device: Empirical and analytical sensitivity analysis with application in post-tensioned frames. *Earthq Eng Struct Dyn*. 52(3):681–702